Animal Cells and Systems
Vol. 15, No. 2, June 2011, 131–138

Taylor & Francis
Taylor & Francis Group

DTNB oxidation effects on T-type Ca^{2+} channel isoforms

Sang-Soo Lee[a], Ho-Won Kang[a], Jin-Yong Park[a,b] and Jung-Ha Lee[a]*

[a]*Department of Life Science, Sogang University, Seoul 121-742, Republic of Korea;* [b]*Department of Neurobiology and Physiology, Northwestern University, Evanston, IL 60208, USA*

(*Received 7 October 2010; received in revised form 6 January 2011; accepted 11 March 2011*)

Redox regulation is one of the ubiquitous mechanisms to modulate ion channels. We here investigated how 5,5′-dithio-bis (2-nitrobenzoic acid), a cysteine specific oxidizing reagent, modulates $Ca_v3.1$ and $Ca_v3.2$ T-type Ca^{2+} channels expressed in *Xenopus* oocytes. Application of the reagent inhibited $Ca_v3.1$ and $Ca_v3.2$ currents in a dose-dependent manner. The oxidizing reagent (1 mM) reduced the peak amplitude of $Ca_v3.1$ and $Ca_v3.2$ currents by ~50% over 2–3 minutes and the decreased currents were fully recovered upon washout of it. The reagent slowed the activation and inactivation kinetics of $Ca_v3.1$, $Ca_v3.2$, and $Ca_v3.3$ channel currents. Notably, the reagent positively shifted both activation and steady-state inactivation curves of $Ca_v3.1$, while it did not those of $Ca_v3.2$. Utilizing chimeric channels from $Ca_v3.1$ and $Ca_v3.2$, we localized the domains III and IV of $Ca_v3.1$ responsible for the positive shifts of channel activation and steady-state inactivation. These findings provide hints relevant to the electrophysiological and molecular mechanisms accounting for the oxidative regulation of T-type channels.

Keywords: T-type Ca^{2+} channel isoforms; 5,5′-dithio-bis-(2-nitrobenzoic acid); oxidation; *Xenopus* oocytes; voltage clamping

Introduction

Calcium influx through T-type Ca^{2+} channels plays essential roles in regulating thalamic oscillation, smooth muscle tone, hormone secretion, acrosome reaction, and cell differentiation (Perez-Reyes and Lory 2006). Molecular cloning and expression studies of T-type channel isoforms exhibited that $Ca_v3.1$ and $Ca_v3.2$ channel currents were rapidly activated and inactivated. In comparison, $Ca_v3.3$ channel currents were characterized to be 5–10-fold slowly activated and inactivated (Lee et al. 1999; Kang et al. 2008). Different electrophysiological properties and expression patterns of the three isoforms suggested their distinctive physiological functions, which were further supported by experimental results obtained from $Ca_v3.1$ or $Ca_v3.2$ knock-out mice (Kim et al. 2001; Chen et al. 2003).

T-type Ca^{2+} channels are basically regulated by membrane potential changes. They have been reported to be also modulated by numerous signaling molecules including G-proteins, protein kinases, and lipids (Kim et al. 2006; Park et al. 2006; Chemin et al. 2007a, b; Hildebrand et al. 2007; Iftinca et al. 2007). Furthermore, it has been reported that signaling pathways leading to redox modification are additional potential factors affecting biophysical properties of ion channels and carrier proteins, consequently regulating critical physiological functions (Zima and Blatter 2006). Previous reports showed that L-type (α_{1C}) calcium channel currents were inhibited by application of oxidizing agents, (2-aminoethyl)methanethiosulfonate (MTSEA), *p*-chloromercuribenzene sulfonic acid (PCMBS), and 2,2′-dithiodipyridine (DTDP), and the reduced currents could be reversed by dithiothreitol (DTT) (Chiamvimonvat et al. 1995; Fearon et al. 1999). Similarly, P/Q-type channel currents were reported to be down-regulated by 5,5′-dithiobis-(2-nitrobenzoic acid) (DTNB), an oxidizing agent (Li et al. 1998).

T-type channel currents recorded in rat sensory neurons were reported to be enhanced by application of DTT, a reducing agent. The $Ca_v3.2$ channel, the main T-type channel isoform in the sensory neurons, was identified to be the target for the DTT-mediated enhancement among three T-type channel isoforms (Joksovic et al. 2006). The DTT-mediated enhancement of $Ca_v3.2$ was discovered to be caused not by reduction, but by chelating off metal ions such as Zn^{2+} and Cu^{2+} from $Ca_v3.2$ (Nelson et al. 2007). In contrast, the same group reported that DTNB, an oxidizing agent, inhibited all T-type channel isoforms with similar potencies and the inhibited currents were recovered by washout of DTNB (Todorovic et al. 2001; Nelson et al. 2005). However, its effects on the biophysical properties of T-type channels have not been characterized. Its interaction region(s) on T-type channels have not been localized, either.

*Corresponding author. Email: jhleem@sogang.ac.kr

ISSN 1976-8354 print/ISSN 2151-2485 online

DOI: 10.1080/19768354.2011.577560
http://www.informaworld.com

Our findings showed that the oxidizing reagent decreased currents through $Ca_v3.1$ and $Ca_v3.2$ channels with similar potencies. It was of interest that DTNB-mediated oxidation significantly shifted the activation and inactivation curves of $Ca_v3.1$ in the positive direction, but scarcely shifted those of $Ca_v3.2$. Characterization of chimeric channels constructed between $Ca_v3.1$ and $Ca_v3.2$ channels suggests that the latter two domains III and IV are more critically involved in the gating shifts of $Ca_v3.1$ than the preceding two domains.

Materials and methods

Chemicals

Most of the chemicals were purchased from Sigma (St. Louis, MO, USA). A DTNB stock solution (600 mM) was made in dimethyl sulfoxide (DMSO) and a series of DTNB solutions (in mM: 0.1, 0.3, 1, 3, 10, and 30) were prepared by diluting the stock solution with 10 mM Ba^{2+} solution just before experiments.

Expression of $Ca_v3.1$, $Ca_v3.2$, and their mutant channels in Xenopus *oocytes*

Preparation of *Xenopus* oocytes was previously reported (Lee et al. 2008). Briefly, ovary lobes were isolated from female *Xenopus laevis* (Xenopus Express, Haute-Loire, France). Isolated lobes were defolliculated by digestion with collagenase (20 mg/ml; SERVA, Heidelberg, Germany) in Ca^{2+}-free Barth's solution (88 mM NaCl, 2.4 mM $NaHCO_3$, 1 mM KCl, 0.82 mM Mg SO_4, pH 7.4) at 20°C for 1 hour. Oocytes in stage V–VI were chosen manually under a dissecting microscope and recovered in incubating at 18°C for several hours. cDNAs encoding $Ca_v3.1$, $Ca_v3.2$ and mutant channels were linearized by *Afl*II and used as templates to synthesize cRNAs using T7 RNA polymerase (Ambion, Austin, TX, USA). The cRNAs were injected into oocytes using a Drummond Nanoject pipette injector (Drummond, Broomall, PA, USA).

Construction of mutant channels

The GenBank accession numbers of rat $Ca_v3.1$ (α_{1G}), human $Ca_v3.2$ (α_{1H}), and rat $Ca_v3.3$ (α_{1I}) are AF027984, AF051946, and AF086827, respectively. The chimeric channels (GGHH and HHGG) between the $Ca_v3.1$ (GGGG) and $Ca_v3.2$ (HHHH) channels were previously reported (Kang et al. 2006). Point mutations were generated using two-step PCR methods. $Ca_v3.1$ mutants (Cys1420Ala, Cys1434Ala, Cys1738Ala and Cys1744Ala) were constructed as follows.

Cys1420Ala

The forward and reverse primers to amplify the upper fragments covering 3495 to 4267 (nucleotide number of $Ca_v3.1$) were 5′-AGCCAGCGGCCGGA GCT-3′ and 5′-CACCCTGAGCCACGAAGAACTTCCCTTTG-3′, respectively. The forward and reverse primers to amplify the lower fragments covering 4251 to 4846 were 5′-CTTCGTGGCTCAGGGTGAGGA-CACCAGG-3′ and 5′-AATTGCAGATCTTCAG AGC-3′. The upper and lower fragments were overlapped and extended by second-step PCR. Cys1420Ala and Cys1434Ala were subcloned into $Ca_v3.1$ pGEM-HEA opened with *Eag*I (3502, $Ca_v3.1$) and *Bgl*II (4836, $Ca_v3.1$).

Cys1434Ala

The forward and reverse primers to amplify the upper fragments covering 3495 to 4309 (nucleotide number of $Ca_v3.1$) were 5′-AGCCAGCGGCCGGA GCT-3′ and 5′-CCTCAGCGGCGTCGGATTTGTTAGTGATG-3′, respectively. The forward and reverse primers to amplify the lower fragments covering 4293 to 4846 were 5′-ATCCGACGCCGCTGAGGCCAGCTACC-GA-3′ and 5′-AATTGCAGATCTTCAGAGC-3′. The cloning method was the same as above.

Cys1738Ala

The forward and reverse primers to amplify the upper fragments covering 4832 to 5222 (nucleotide number of $Ca_v3.1$) were 5′-TGAAGATCTGCAATTACATC-3′ and 5′-GTCTCATCAGCCTCCAGGTCTCCAAA-GAG-3′, respectively. The forward and reverse primers to amplify the lower fragments covering 5205 to 3′-polylinker were 5′-CCTGGAGGCTGATGAGACA-CACCCTTGT-3′ and 5′-GACTCTCCGGAAGTT CTG-3′. The upper and lower fragments were overlapped and extended by second-step PCR. Cys1738Ala and Cys1744Ala were subcloned into $Ca_v3.1$ pGEM-HEA opened with *Bgl*II (4836, $Ca_v3.1$) and *BspE*I (3′-polylinker).

Cys1744Ala

The forward and reverse primers to amplify the upper fragments covering 4832 to 5239 (nucleotide number of $Ca_v3.1$) were 5′-TGAAGATCTGCAATTACATC-3′ and 5′-AGCCCTCAGCAGGGTGTGTCTCATCACA-3′, respectively. The forward and reverse primers to amplify the lower fragments covering 5223 to 3′-polylinker were 5′-ACACCCTGCTGAGGGCTTGG GTCGGCAT-3′ and 5′-GACTCTCCGGAAGTTCTG -3′. The cloning method was the same as above.

Electrophysiological recording and data analysis

Barium inward currents were measured using a two-microelectrode voltage clamp amplifier (OC-725C, Warner Instruments, Hamden, CT, USA) between 3 and 5 days after cRNA injection in oocytes. Glass capillaries were pulled into microelectrodes to produce a resistance of 0.3–1.0 MΩ. After picking an oocyte with microelectrodes filled with 3 M KCl in SOS (standard oocyte solution), 10 mM Ba^{2+} solution (10 mM $Ba(OH)_2$, 90 mM NaOH, 5 mM HEPES, 1 mM KOH, pH 7.4 with methanesulfonic acid) was perfused into a chamber and currents were recorded. The currents were low-pass filtered at 1 kHz and acquired at 5 kHz using the pClamp system (Digidata 1322A and pClamp 8; Axon instruments, Foster City, CA, USA). Peak currents and exponential fits to currents were analyzed using Clampfit 8.0 software and the data were graphically presented with Prism software (GraphPad, San Diego, CA, USA). Data are given as mean ± SEM. Differences were tested for significance using Student's unpaired *t* test.

Results

Inhibitory effects of DTNB on T-type channel isoforms

Robust inward Ba^{2+} currents were evoked from oocytes injected with $Ca_v3.1$ or $Ca_v3.2$ channel cRNA in response to a test potential of −20 mV from a holding potential of −90 mV (Figures 1 and 2). Electrophysiological properties of $Ca_v3.1$ and $Ca_v3.2$ channels characterized in a 10 mM Ba^{2+} solution were similar to those previously reported (Table 1; Lee et al. 1999). In contrast, no inward currents were detected from oocytes injected with 0.1 M KCl (data not shown).

We first examined how $Ca_v3.1$ and $Ca_v3.2$ T-type channels were regulated by application of DTNB, a cysteine-specific oxidizing agent. Superfusion of serial DTNB solutions onto an oocyte expressing $Ca_v3.1$ channels inhibited the peak current amplitude of $Ca_v3.1$ in a concentration dependent manner ($n=5$; Figure 1A,C). The IC_{50} value was estimated to be 1.02 ± 0.08 mM. $Ca_v3.2$ currents evoked by a test potential of −20 mV were also inhibited by the oxidizing agent in a dose-dependent manner (IC_{50} value for $Ca_v3.2 = 1.04\pm0.07$ mM, $n=5$; Figure 1B, D). When superfused with 1 mM DTNB solution, currents through $Ca_v3.1$ or $Ca_v3.2$ channels were reduced to ~50% in amplitude ($n=9$; Figure 1E, F). When the time courses of DTNB inhibition for $Ca_v3.1$ and $Ca_v3.2$ currents are plotted and fitted with single exponential equation, the time constants of DTNB inhibition are estimated to be 70 ± 4 and 78 ± 3 sec, respectively. The DTNB-mediated inhibition of $Ca_v3.1$ and $Ca_v3.2$ currents was fully recovered by washing it with 10 mM Ba^{2+} solution.

Similarly, application of DTNB dose-dependently inhibited the peak current amplitude of $Ca_v3.3$ (IC_{50} value for $Ca_v3.3 = 1.03\pm0.09$ mM, $n=4$, Supplementary Figure 1). Current-voltage relationships, activation and inactivation curves, and current kinetics of $Ca_v3.3$ before and after 1 mM DTNB treatment are compared in Supplementary Figure 1 and the DTNB

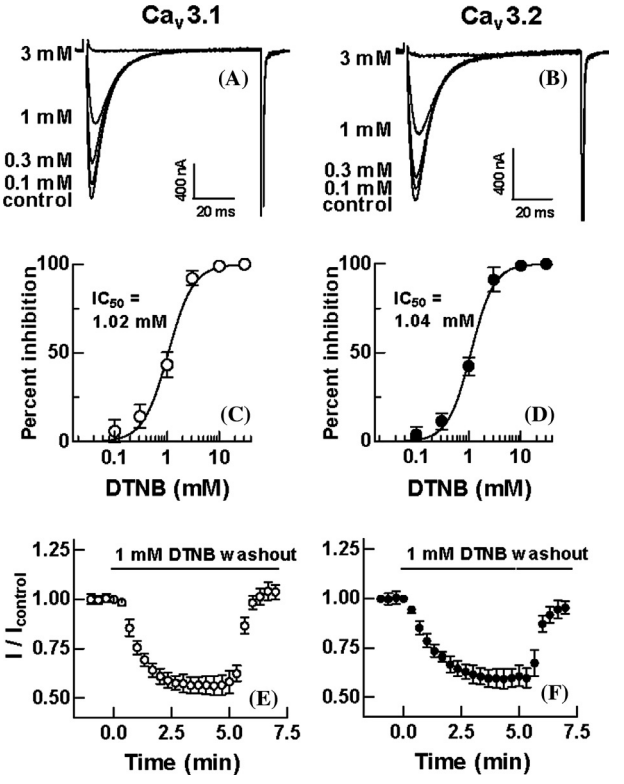

Figure 1. DTNB inhibition effects on $Ca_v3.1$ and $Ca_v3.2$ channel currents. Currents were evoked by a test potential of −20 mV from a holding potential of −90 mV every 20 sec. A and B, representative current traces of $Ca_v3.1$ (A) and $Ca_v3.2$ (B) channels in response to application of serial DTNB solutions. The currents before and after DTNB inhibition were shown in overlap. C and D, dose-response curves. $Ca_v3.1$ (C) and $Ca_v3.2$ (D) currents were normalized to the peak current measured before application of DTNB solutions, and the percentages were plotted against DTNB concentrations. The smooth curves were obtained from fitting the data with the Hill equation: $B=(1+IC_{50}/(DTNB)^n)^{-1}$, where B is the normalized block, IC_{50} is the concentration of DTNB required for half maximal inhibition, and *n* is the Hill coefficient. The IC_{50} values for $Ca_v3.1$ and $Ca_v3.2$ channels were 1.02 ± 0.08 and 1.04 ± 0.07 mM, respectively (mean ± SEM, $n=5$). E and F, time courses of the DTNB-mediated inhibition of $Ca_v3.1$ and $Ca_v3.2$ currents. $Ca_v3.1$ (E) and $Ca_v3.2$ (F) currents were normalized to the peak current amplitude before 1 mM DTNB treatment and their normalized ratios (mean ± SEM, $n=9$) were plotted against time.

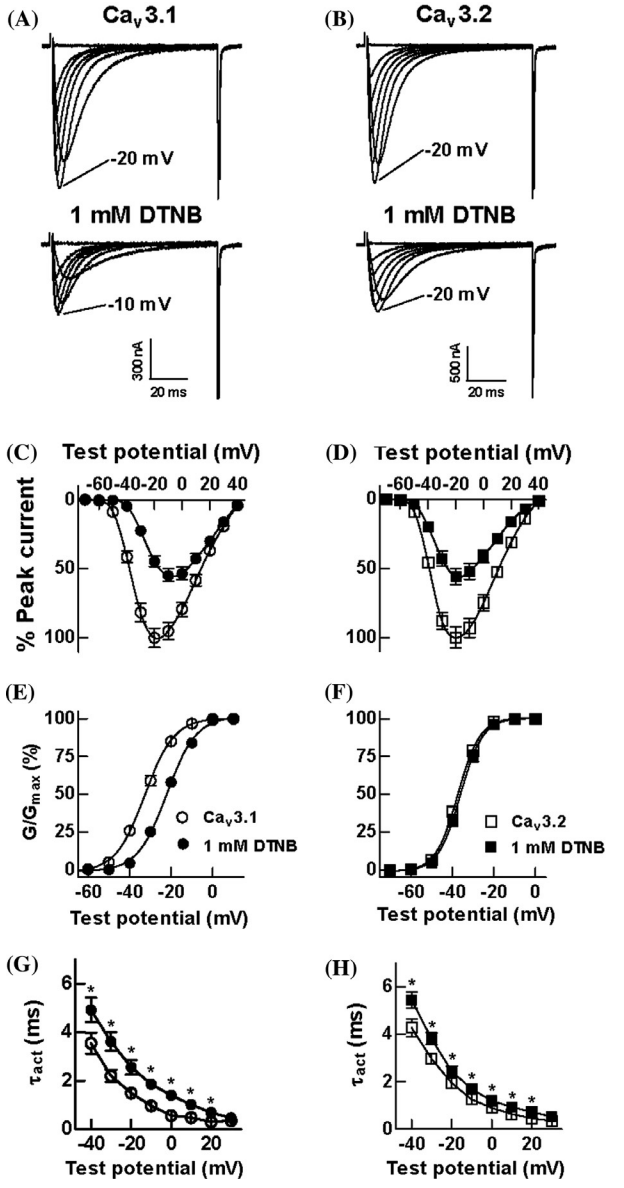

Figure 2. DTNB effects on activation properties of $Ca_v3.1$ and $Ca_v3.2$ channels. A and B, representative $Ca_v3.1$ (A) and $Ca_v3.2$ (B) currents before (upper) and after (lower) 1 mM DTNB treatment. Currents were elicited by serial test potentials of −70 to +40 mV by 10 mV increments from a holding potential of −90 mV. Currents elicited by test potentials of −70, −30, −20, −10, 0, 10, and 20 mV are represented. C and D, current-voltage (*I–V*) relationships of $Ca_v3.1$ (C) and $Ca_v3.2$ (D) channels before (○, $Ca_v3.1$; □, $Ca_v3.2$) and after (●, $Ca_v3.1$; ■, $Ca_v3.2$) application of 1 mM DTNB for 5 min. E and F, activation curves of $Ca_v3.1$ (E) and $Ca_v3.2$ (F) channels before and after application of 1 mM DTNB. They were obtained by plotting chord conductances (*G*), calculated by dividing the current amplitude by driving force, normalized to the maximum and fitted to the Boltzmann equation. G and H, activation time constant (τ_{act}) of $Ca_v3.1$ (G) and $Ca_v3.2$ (H) currents. Activation time constants were derived from fitting individual current traces with two exponentials. Data are represented as mean ± SEM ($n = 5–8$).

Table 1. Biophysical properties of the $Ca_v3.1$, $Ca_v3.2$ and chimeric channels in the absence and presence of 1 mM DTNB.

	IC_{50}	V_{50act}		$V_{50inact}$		τ_{act}(−20 mV)		τ_{inact}(−20 mV)	
		Control	+1 mM DTNB	Control	+1 mM DTNB	Control	+1 mM DTNB	Control	+1 mM DTNB
$Ca_v3.1$ (GGGG)	1.02 ± 0.08	−32.6 ± 0.3	−22.1 ± 0.5[b]	−59.7 ± 0.3	−50.5 ± 0.2[b]	1.48 ± 0.13	2.56 ± 0.32[a]	7.42 ± 0.42	10.01 ± 0.54[a]
$Ca_v3.2$ (HHHH)	1.04 ± 0.07	−37.3 ± 0.3	−36.3 ± 0.4	−62.1 ± 0.3	−60.8 ± 0.4	1.94 ± 0.09	2.44 ± 0.21[a]	7.44 ± 0.37	11.24 ± 0.47[a]
GGHH	1.05 ± 0.11	−36.5 ± 0.6	−34.7 ± 0.5	−58.8 ± 0.4	−56.5 ± 0.2	1.40 ± 0.06	1.88 ± 0.16[a]	7.54 ± 0.60	9.61 ± 0.70[a]
HHGG	1.06 ± 0.13	−33.8 ± 0.5	−25.9 ± 0.6[b]	−60.3 ± 0.7	−54.3 ± 0.6[a]	1.86 ± 0.32	2.70 ± 0.20[a]	8.77 ± 0.92	12.50 ± 0.88[a]

IC_{50} values were estimated from fitting data with the Hill's equation. Activation and inactivation curves were fitted with the Boltzmann equation. All data are shown with mean ± SEM (n = 4–9). Significant differences before and after DTNB treatment were evaluated by Student *t*-test: [a], $p < 0.05$; [b], $p < 0.01$.

effects on $Ca_v3.3$ are summarized in Supplementary Table 1.

DTNB effects on T-type channel activation

We characterized how DTNB affects the activation properties of $Ca_v3.1$ or $Ca_v3.2$ channels. *I–V* relationships were obtained using serial depolarizing potentials from −70 mV to +40 mV in 10 mV increments. Representative current traces of $Ca_v3.1$ and $Ca_v3.2$ before and after application of 1 mM DTNB are shown in Figure 2A and B. Comparison of the *I–V* curves showed that application of 1 mM DTNB positively shifted the *I–V* relationship of $Ca_v3.1$, while it scarcely shifted that of $Ca_v3.2$ ($n=6$; Figure 2C, D). Consistently, analysis of chord conductance showed that DTNB (1 mM) shifted the activation curve of $Ca_v3.1$ in the positive direction by 10.5 mV (V_{50act} values before and after 1 mM DTNB treatment = -32.6 ± 0.3 vs -22.1 ± 0.5 mV; $n=5$; $P<0.01$), whereas it did not significantly that of $Ca_v3.2$ ($V_{50act}=-37.3\pm0.3$ vs -36.3 ± 0.4 mV; $n=5$; Figure 2E, F, Table 1). We also examined whether DTNB can affect the activation time constants of $Ca_v3.1$ and $Ca_v3.2$ channel currents. Analysis of $Ca_v3.1$ and $Ca_v3.2$ current traces before and after DTNB treatment revealed that the activation time constants of both channels were significantly decelerated over most of the test potentials examined ($n=5$; Figure 2G, H, Table 1).

DTNB effects on T-type channel inactivation

We subsequently examined how DTNB affects the steady-state inactivation of $Ca_v3.1$ and $Ca_v3.2$ channels. Representative current traces of $Ca_v3.1$ and $Ca_v3.2$ recorded during voltage steps to −20 mV from various prepulse potentials from −100 mV to −40 mV are shown before and after 1 mM DTNB treatment (Figure 3A, B). Analysis of the steady-state inactivation curves of $Ca_v3.1$ revealed that the steady-state inactivation curve of $Ca_v3.1$ was positively shifted by 9.2 mV ($V_{50inact}$ before and after 1 mM DTNB treatment = -59.7 ± 0.3 vs -50.5 ± 0.2 mV; $n=6$; $P<0.01$), whereas that of $Ca_v3.2$ was not significantly shifted ($V_{50inact}=-62.1\pm0.3$ vs -60.8 ± 0.4; $n=5$; Figure 3C, D, Table 1). In addition, analysis of $Ca_v3.1$ and $Ca_v3.2$ current traces evoked by a serial depolarizing voltage protocol showed that the inactivation time constants of both channels were significantly decelerated over most of the potentials by the oxidizing reagent ($n=5$ or 6; Figure 3E, F, Table 1). We further examined whether DTNB can affect the recovery properties of both channels. It turned out that the oxidizing agent little affected the recovery of either T-type channel (data not shown).

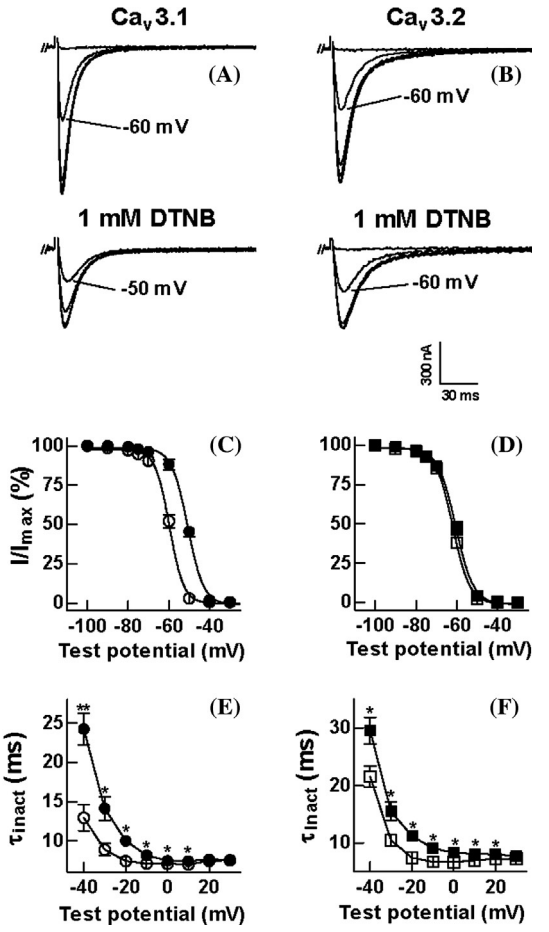

Figure 3. DTNB effects on inactivation properties of $Ca_v3.1$ and $Ca_v3.2$ channels. A and B, representative current traces of $Ca_v3.1$ (A) and $Ca_v3.2$ (B) channels before (upper) and after (lower) 1 mM DTNB treatment. Steady-state inactivation properties were tested during a voltage step to −20 mV following prepulse potentials varying from −100 to −40 mV for 10 sec. C and D, Steady-state inactivation curves of $Ca_v3.1$ (G) and $Ca_v3.2$ (H) before and after application of 1 mM DTNB. E and F, inactivation time constants (τ_{inact}) of $Ca_v3.1$ (E) and $Ca_v3.2$ (F) channels. Inactivation constants were obtained from fitting currents with two exponentials. Data are represented as mean ± SEM ($n=5$ or 6).

Localization of region(s) contributing to the DTNB-mediated gating shift of $Ca_v3.1$

DTNB inhibited $Ca_v3.1$ and $Ca_v3.2$ channel currents with similar potencies. But the reagent caused the activation and steady-state inactivation curves of only $Ca_v3.1$ to positively shift, but not those of $Ca_v3.2$ channels. We attempted to localize the structural region(s) responsible for the DTNB-mediated gating shifts of $Ca_v3.1$ channels. Activation and steady-state inactivation of two chimeric channels (GGHH and HHGG) with swapped halves of $Ca_v3.1$ (GGGG) and $Ca_v3.2$ (HHHH) channels were examined (Figure 4A; Kang et al. 2006). Analysis of the data showed that

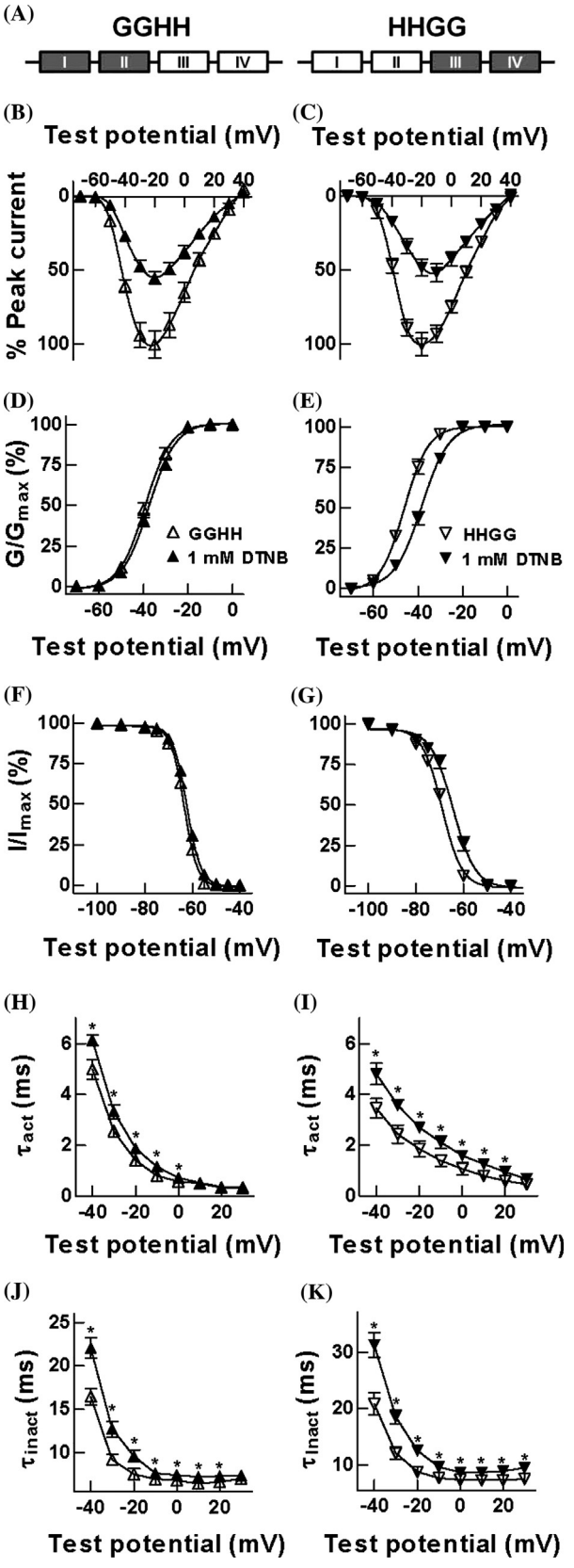

Figure 4. DTNB effects on GGHH and HHGG chimeric channels. A, schematic diagrams of GGHH and HHGG chimeras derived from $Ca_v3.1$ and $Ca_v3.2$ channels. Gray boxes indicate the domains from $Ca_v3.1$ (GGGG), while white boxes indicate from $Ca_v3.2$ (HHHH). B and C, normalized *I–V* relationships of GGHH (B) and HHGG (C) before (△, GGHH; ▽, HHGG) and after (▲, GGHH; ▼, HHGG) 1 mM DTNB treatment for 5 min. Voltage steps were depolarized from −70 to +40 mV by 10 mV increments with a holding potential of −90 mV. D and E, activation curves of GGHH (D) and HHGG (E). F and G, steady-state inactivation curves of GGHH (F) and HHGG (G) channels. H and I, activation time constants (t_{act}) of GGHH (H) and HHGG (I) chimeric channels before (△, GGHH; ▽, HHGG) and after (▲, GGHH; ▼, HHGG) 1 mM DTNB treatment. J and K, inactivation time constants (τ_{inact}) of GGHH (J) and HHGG (K) channels before and after 1 mM DTNB treatment. Data are given as mean ± SEM ($n = 4$–7).

DTNB (1 mM) positively shifted the activation curve of HHGG chimera by 7.9 mV and its inactivation curve by 6 mV (Figure 4E, G, Table 1). In contrast, application of DTNB did not significantly shift the activation or inactivation curves of GGHH ($n = 5$–7; Figure 4D, F, Table 1). These findings suggest that the domains III and IV of $Ca_v3.1$ may contain structural element(s) contributing to the positive shifts caused by DTNB.

We next looked for cysteine residues contributing to the DTNB-mediated gating shift and/or inhibition in the post-half structure. We chose four cysteine residues (Cys1420, Cys1434, Cys1738, and Cys1744) at the S5–pore linkers of the domains III and IV and individually mutated them into alanine residues (Supplementary Figure 2A). When attempts were made to express Cys1420Ala, Cys1434Ala, Cys1738Ala, and Cys1744Ala mutants in oocytes, all of the mutant channels produced robust barium currents in response to a test potential of −20 mV from a holding potential of −90 mV. Application of 1 mM DTNB inhibited currents through the four Cys mutant channels with similar potencies. The IC_{50} values for the four mutants are about 1 mM. Analysis of activation and inactivation curves of the Cys mutant channels showed that DTNB positively shifted their activation and inactivation curves, similarly to the wild-type $Ca_v3.1$ (Supplementary Figure 2). These results suggest that Cys1420, Cys1434, Cys1738, and Cys1744 are not involved in the positive shifts by DTNB. The biophysical effects of the mutant channels caused by 1 mM DTNB are summarized in Supplementary Table 1.

Discussion

We here report that DTNB inhibited the current amplitude of $Ca_v3.1$, $Ca_v3.2$, and $Ca_v3.3$ T-type Ca^{2+} channels with similar potencies and de-accelerated their

activation and inactivation time constants. Notably, the oxidizing reagent differentially regulated the activation and steady-state inactivation curves of $Ca_v3.1$ and $Ca_v3.2$ as follows. The activation and steady-state inactivation curves of $Ca_v3.1$ and $Ca_v3.3$ were positively shifted, whereas those of $Ca_v3.2$ were little shifted by the oxidizing agent. The chimeric channel experiments suggest the domains III and IV of $Ca_v3.1$ to be more responsible for the positive shifts of channel activation and steady-state inactivation than the domains I and II. Point mutation experiments of Cys1420, Cys1434, Cys1738, and Cys1744 at the pore regions of the domains III and IV suggest that the cysteine residues are not likely to be responsible for the positive shifts. Therefore, it remains to be further investigated whether other cysteine residues spreading over the domains III and IV of $Ca_v3.1$ channels are involved in the DTNB-mediated positive shifts.

Application of 1 mM DTNB positively shifted activation and inactivation curves of wild-type $Ca_v3.1$ (GGGG) by 10.5 mV and 9.2 mV, respectively. In comparison, the oxidizing reagent shifted activation and inactivation curves of HHGG chimera by 7.0 mV and 6.0 mV, respectively, indicating that the shifting levels (ΔV_{act} and ΔV_{inact}) of HHGG caused by DTNB are slightly less than those of wild-type $Ca_v3.1$ (Student's unpaired t test, $P < 0.05$). These results suggest that the post-half of $Ca_v3.1$ (GGGG) may play more important roles in the gating shifts than the pre-half of it. In comparison, Karmazinova and her colleagues recently reported that Cys residues at the external loop connecting S5 and pore in domain I of $Ca_v3.1$ participate critically in DTNB effects (Karmazinova et al. 2010). Combining our results with the report suggests that cysteine residues contributing to the DTNB effect are spread over multiple regions of the $Ca_v3.1$ channel.

In addition, they also reported that DTNB shifted the current activation curve of wild-type $Ca_v3.1$ channels in the hyperpolarizing direction. This is different from our data showing that DTNB shifted $Ca_v3.1$ channel gating in a positive direction. The contradictory results might come from several different experimental conditions. For example, they tested DTNB effects on mouse $Ca_v3.1$ tagged with EGFP in HEK293 cells, while we studied DTNB effects on rat $Ca_v3.1$ in *Xenopus* oocytes. Alternatively, their result that DTNB negatively shifted the current activation curve of wild-type $Ca_v3.1$ channels might come from improper data analysis. For example, the reported I–V data showed that the peak current amplitude of $Ca_v3.1$ at a test potential of -60 mV was about two-fold increased by DTNB, while the peak current amplitude at most of the other test potentials was decreased. The data showing that the DTNB increased the current amplitude at a low test potential(s) is likely to produce the questionable result that DTNB negatively shifted the activation curve.

DTNB is known to be a non-permeable agent specifically oxidizing cysteines. The reagent is thus supposed to react with thiol groups of cysteine residues exposed to the extracellular face, some of which are capable of forming disulfide bonds between neighboring cysteines (Britto et al. 2005; Joksovic et al. 2006). Analysis of the amino acid sequence and topology of the domains III and IV of rat $Ca_v3.1$ suggests multiple candidate cysteine residues being exposed to the extracellular side. Point mutation experiments of Cys1420, Cys1434, Cys1738, and Cys1744 at the S5–pore linkers of the domains III and IV suggest that none of them participate in the DTNB-mediated positive shifts of activation and inactivation curves. It remains to be further investigated whether other cysteine residues, including Cys1614 at the S1–S2 linker, and Cys1783 and Cys1789 at the pore–S6 linker of the domain IV, are involved in the DTNB-mediated gating shift.

In summary, we found that DTNB inhibited $Ca_v3.1$, $Ca_v3.2$, and $Ca_v3.3$ T-type channel activities with similar potencies. The oxidant positively shifted the gating of $Ca_v3.1$ and $Ca_v3.3$, but did not that of $Ca_v3.2$, suggesting that T-type channel isoforms can be differentially modulated by oxidative conditions. In pathophysiological conditions such as ischemia, for example, oxidation of T-type channel isoforms by free radicals may similarly reduce calcium influx through T-type channel isoforms, but differently modulate the gating and inactivation properties of T-type channel isoforms, which may be coupled with the different levels of cell damage caused by external calcium entry.

Acknowledgements

This work was supported by the Korea Science and Engineering Foundation (KOSEF) grant (SRC, 2008-0062410), Priority Research Centers Program (2009-0093822) and Basic Science Research Program (2009-0087964) through the National Research Foundation of Korea.

References

Britto PJ, Knipling L, McPhie P, Wolff J. 2005. Thiol-disulfide interchange in tubulin: kinetics and the effect on polymerization. Biochem J. 389:549–558.

Chemin J, Mezghrani A, Bidaud I, Dupasquier S, Marger F, Barrere C, Nargeot J, Lory P. 2007a. Temperature-dependent modulation of Cav3 T-type calcium channels by protein kinases C and A in mammalian cells. J Biol Chem. 282:32710–3218.

Chemin J, Nargeot J, Lory P. 2007b. Chemical determinants involved in anandamide-induced inhibition of T-type calcium channels. J Biol Chem. 282:2314–2323.

Chen CC, Lamping KG, Nuno DW, Barresi R, Prouty SJ, Lavoie JL, Cribbs LL, England SK, Sigmund CD, Weiss RM, Williamson RA, Hill JA, Campbell KP. 2003. Abnormal coronary function in mice deficient in α_{1H} T-type Ca^{2+} channels. Science. 302:1416–1418.

Chiamvimonvat N, O'Rourke B, Kamp TJ, Kallen RG, Hofmann F, Flockerzi V, Marban E. 1995. Functional consequences of sulfhydryl modification in the pore-forming subunits of cardiovascular Ca^{2+} and Na^{+} channels. Circ Res. 76:325–334.

Fearon IM, Palmer ACV, Balmforth AJ, Ball SG, Varadi G, Peers C. 1999. Modulation of recombinant human cardiac L-type Ca^{2+} channel α_{1C} subunits by redox agents and hypoxia. J Physiol. 514:629–637.

Hildebrand ME, David LS, Hamid J, Mulatz K, Garcia E, Zamponi GW, Snutch TP. 2007. Selective inhibition of $Ca_v3.3$ T-type calcium channels by $G_{\alpha/11}$-coupled muscarinic acetylcholine receptors. J Biol Chem. 282:32710–32718.

Iftinca M, Hamid J, Chen L, Varela D, Tadayonnejad R, Altier C, Turner RW, Zamponi GW. 2007. Regulation of T-type calcium channels by Rho-associated kinase. Nat. Neurosci. 10:854–860.

Joksovic PM, Nelson MT, Jevtovic-Todorovic V, Patel MK, Perez-Reyes E, Campbell KP, Chen CC, Todorovic SM. 2006. $Ca_v3.2$ is the major molecular substrate for redox regulation of T-type Ca^{2+} channels in the rat and mouse thalamus. J Physiol. 574:415–430.

Kang HW, Park JY, Jeong SW, Kim JA, Moon HJ, Perez-Reyes E, Lee JH. 2006. A molecular determinant of nickel inhibition in Cav3.2 T-type calcium channels. J Biol Chem. 281:4823–4830.

Kang HW, Park JY, Lee JH. 2008. Distinct contributions of different structural regions to the current kinetics of the $Ca_v3.3$ T-type Ca^{2+} channel. Biochim Biophys Acta. 1778:2740–2748.

Kang HW, Vitko I, Lee SS, Perez-Reyes E, Lee JH. 2010. Structural determinants of the high affinity extracellular zinc binding site on $Ca_v3.2$ T-type calcium channels. J Biol Chem. 285:3271–3281.

Karmazinova M, Beyl S, Stary-Weinzinger A, Suwattanasophon C, Klugbauer N, Hering S, Lacinova L. 2010. Cysteines in the loop between IS5 and the pore helix of CaV3.1 are essential for channel gating. Pflugers Arch. 460:1015–1028.

Kim D, Song I, Keum S, Lee T, Jeong MJ, Kim SS, McEnery MW, Shin HS. 2001. Lack of the burst firing of thalamocortical relay neurons and resistance to absence seizures in mice lacking α_{1G} T-type Ca^{2+} channels. Neuron. 31:35–45.

Kim JA, Park JY, Kang HW, Huh SU, Jeong SW, Lee JH. 2006. Augmentation of $Ca_v3.2$ T-type calcium channel activity by cAMP-dependent protein kinase A. J Pharmacol Exp Ther. 318:230–237.

Lee JH, Daud AN, Cribbs LL, Lacerda AE, Pereverzev A, Klockner U, Schneider T, Perez-Reyes E. 1999. Cloning and expression of a novel member of the low voltage-activated T-type calcium channel family. J Neurosci. 19:1912–1929.

Lee SS, Park YM, Kang HW, Bang H, Jeong SW, Lee JH. 2008. Differential expression of four $Ca_v3.1$ splice variants in the repeat III–IV loop. Anim Cells Syst. 12:137–141.

Lee WY, Orestes P, Latham J, Naik AK, Nelson MT, Vitko I, Perez-Reyes E, Todorovic VJ, Todorovic SM. 2009. Molecular mechanisms of lipoic acid modulation of T-type calcium channels in pain pathway. J Neurosci. 29:9500–9509.

Li A, Segui J, Heinemann SH, Hoshi T. 1998. Oxidation regulates cloned neuronal voltage-dependent Ca^{2+} channels expressed in Xenopus oocytes. J Neurosci. 18:6740–6747.

Nelson MT, Joksovic PM, Perez-Reyes E, Todorovic SM. 2005. The endogenous redox agent L-cysteine induces T-type Ca^{2+} channel-dependent sensitization of a novel subpopulation of rat peripheral nocieptos. J Neurosci. 25:8766–8775.

Nelson MT, Woo J, Kang HW, Vitko I, Barrett PQ, Perez-Reyes E, Lee JH, Shin HS, Todorovic SM. 2007. Reducing agents sensitize C-type nociceptors by relieving high-affinity zinc inhibition of T-type calcium channels. J Neurosci. 27:8250–8260.

Park JY, Kang HW, Moon HJ, Huh SU, Jeong SW, Soldatov NM, Lee JH. 2006. Activation of protein kinase C augments T-type Ca^{2+} channel activity without changing channel surface density. J Physiol. 577:513–523.

Perez-Reyes E, Lory P. 2006. Molecular biology of T-type calcium channels. CNS Neurol Disord Drug Targets. 5:605–609.

Todorovic SM, Jevtovic-Todorovic V, Meyenburg A, Mennerick S, Perez-Reyes E, Romano C, Olney JW, Zorumski CF. 2001. Redox modulation of T-type calcium channels in rat peripheral nociceptors. Neuron. 31:75–85.

Zima AV, Blatter LA. 2006. Redox regulation of cardiac channels and transporters. Cardiovasc Res. 71:310–321.